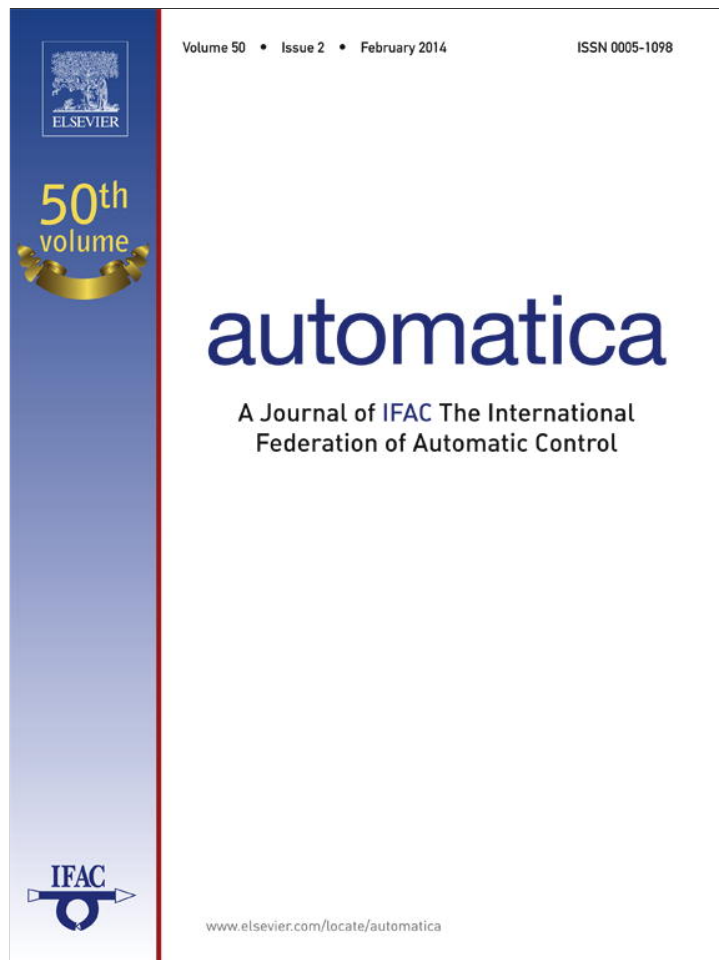


Provided for non-commercial research and education use.
Not for reproduction, distribution or commercial use.



This article appeared in a journal published by Elsevier. The attached copy is furnished to the author for internal non-commercial research and education use, including for instruction at the authors institution and sharing with colleagues.

Other uses, including reproduction and distribution, or selling or licensing copies, or posting to personal, institutional or third party websites are prohibited.

In most cases authors are permitted to post their version of the article (e.g. in Word or Tex form) to their personal website or institutional repository. Authors requiring further information regarding Elsevier's archiving and manuscript policies are encouraged to visit:

<http://www.elsevier.com/authorsrights>



Contents lists available at ScienceDirect

Automatica

journal homepage: www.elsevier.com/locate/automatica

Brief paper

Potential and optimal control of human head movement using Tait–Bryan parametrization[☆]



Indika Wijayasinghe^a, Justin Ruths^f, Ulrich Büttner^{b,d}, Bijoy K. Ghosh^{a,1}, Stefan Glasauer^{b,d}, Olympia Kremmyda^c, Jr-Shin Li^e

^a Department of Mathematics and Statistics, Texas Tech University, Lubbock, TX, USA

^b Integrated Research and Treatment Center for Vertigo IFB-LMU, University Clinic Munich, Munich, Germany

^c Department of Neurology, Ludwig-Maximilians University, Munich, Germany

^d Center of Sensorimotor Research, Ludwig-Maximilians University, Munich, Germany

^e Department of Electrical and Systems Engg., Washington University, Saint Louis, USA

^f Engineering Systems & Design Pillar, Singapore University of Technology and Design, Singapore

ARTICLE INFO

Article history:

Received 22 May 2012

Received in revised form

4 September 2013

Accepted 9 October 2013

Available online 6 January 2014

Keywords:

Head movement

Donders' surface

Tait–Bryan parametrization

Euler Lagrange's equation

Potential control

Optimal control

ABSTRACT

Human head movement can be looked at, as a rotational dynamics on the space $SO(3)$ with constraints that have to do with the axis of rotation. Typically the axis vector, after a suitable scaling, is assumed to lie in a surface called Donders' surface. Various descriptions of Donders' surface are in the literature and in this paper we assume that the surface is described by a quadratic form. We propose a Tait–Bryan parametrization of $SO(3)$, that is new in the head movement literature, and describe Donders' constraint in these parameters. Assuming that the head is a perfect sphere with its mass distributed uniformly and rotating about its own center, head movement models are constructed using classical mechanics. A new potential control method is described to regulate the head to a desired final orientation. Optimal head movement trajectories are constructed using a pseudospectral method, where the goal is to minimize a quadratic cost function on the energy of the applied control torques. The model trajectories are compared with measured trajectories of human head movement.

© 2013 Elsevier Ltd. All rights reserved.

1. Introduction

Neurologists, physiologists and engineers have been interested in modeling and control of the eye since 1845 with notable studies conducted by Donders (1848), Listing (1845) and von Helmholtz (1866). Specifically, it has been observed that the oculomotor system chooses just one angle of ocular torsion for any one gaze direction (see Donders, 1848). Since its discovery, Donders' law has also been applied to the head (see Ceylan, Henriques, Tweed, &

Crawford, 2000), which is mechanically able to rotate torsionally, but which normally adopts just one torsional angle for any one facing direction; see Straumann, Haslwanter, Hepp–Reymond, and Hepp (1991) and Glenn and Vilis (1992). A geometric consequence of Donders' law is that the three dimensional vectors that represent the 'rotation vectors' of the head are not spread out in a 3-D volume but instead fall in a single two-dimensional surface known as Donders' surface. It has been further proposed, see Glenn and Vilis (1992), Medendorp, Melis, Gielen, and Gisbergen (1998), Misslisch, Tweed, and Vilis (1998), Radau, Tweed, and Vilis (1994), Theeuwes, Miller, and Gielen (1993) and Tweed, Glenn, and Vilis (1995), that Donders' law follows what is known as Fick's strategy. According to this strategy, Donders' surface is a saddle-shaped surface, with non-zero torsional components at oblique facing directions, obtained by mildly twisting a plane. Donders' surfaces of various shapes are shown in Fig. 1, obtained from experimentally recorded head movement data.

We begin by revisiting Donders' law following the Fick gimbal strategy (see Fick, 1858). The Fick strategy of human head movement is to rotate the head in such a way that the line joining the center of the two eyes remain horizontal at all times, assuming that the head orientation initially satisfies this constraint. A typical

[☆] The paper is based upon work supported in part by the National Science Foundation under Grant No. 1029178. Part of this research is also supported by BMBF Grant No. 01E00901. The material in this paper was partially presented at the 18th IFAC World Congress, August 28–September 2, 2011, Milan, Italy. This paper was recommended for publication in revised form by Associate Editor Warren E. Dixon under the direction of Editor Andrew R. Teel.

E-mail addresses: indika.wijayasinghe@ttu.edu (I. Wijayasinghe), justinruths@sutd.edu.sg (J. Ruths), Ulrich.Buettner@med.uni-muenchen.de (U. Büttner), bijoy.ghosh@ttu.edu (B.K. Ghosh), s.glasauer@lrz.uni-muenchen.de (S. Glasauer), Olympia.Kremmyda@med.uni-muenchen.de (O. Kremmyda), jsli@ese.wustl.edu (J.-S. Li).

¹ Tel.: +1 806 742 2566; fax: +1 806 742 1112.

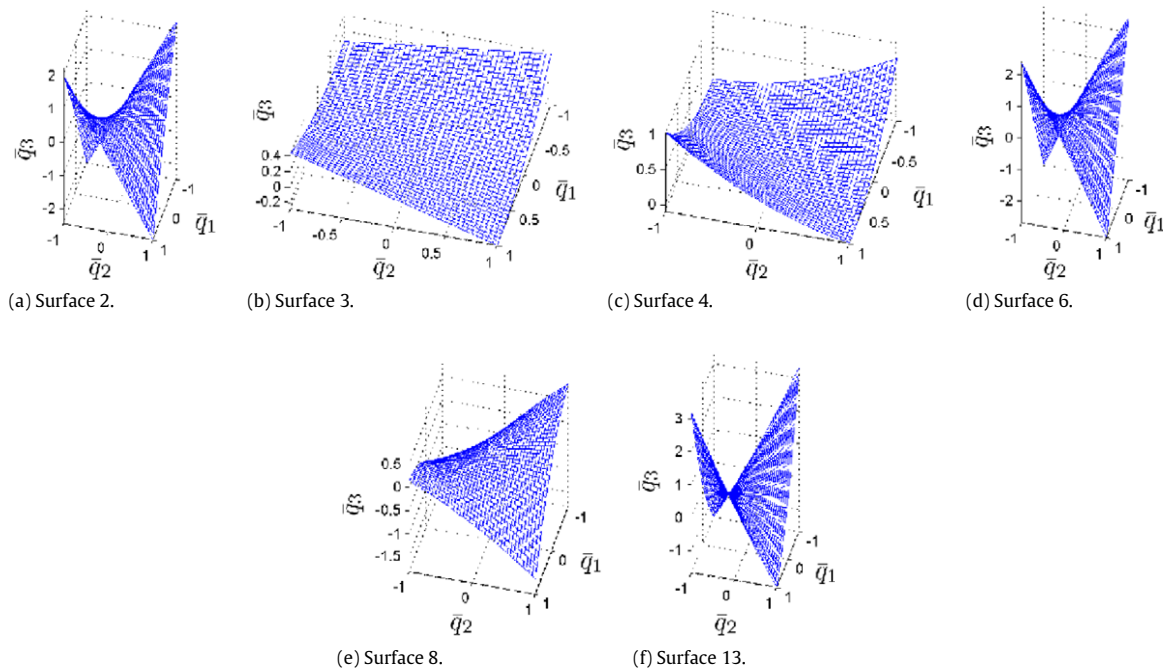


Fig. 1. Using collected data on human head orientations, six Donders' surfaces displayed in this figure are obtained by regressing the head orientation points represented as unit quaternions. The three coordinates are the scaled coordinates \bar{q}_1 , \bar{q}_2 and \bar{q}_3 .

gimbal system has two axes of rotations, where the assumption is that the first axis is fixed and the second axis rotates with the head, when the head rotates about the first axis. Subsequently, the head also rotates about the second axis. We assume that the fixed axis is the vertical axis, which is perpendicular to the ground and passes through the center of the head. The initial orientation of the second axis is horizontal and is parallel to the line joining the two eyes, also passing through the center of the head. We denote the anticlockwise rotation angle about the fixed (yaw) axis by ϕ_1 , and the anticlockwise rotation angle about the nested horizontal (pitch) axis by ϕ_2 . The roll is assumed to be zero and the final orientation of the head is a combination of the two rotations, yaw and pitch. In this paper, the Fick gimbal strategy is modified by introducing a non-zero roll as a function of yaw and pitch. Let us consider a third axis, initially along the line of gaze perpendicular to the vertical and horizontal axes. We assume that the third axis rotates with respect to the first two axes by angles ϕ_1 and ϕ_2 respectively. Finally, we assume that the head rotates anticlockwise by an angle ϕ_3 with respect to the nested third (roll) axis. A specific rotation in $SO(3)$ can be parameterized by the three angles ϕ_1 , ϕ_2 and ϕ_3 , and these are called the Tait–Bryan angles. Donders' surface is implemented as a constraint on the three angles, to be described later in this paper. The yaw, pitch and roll are respectively the axes 1, 2 and 3 in Fig. 2. This figure also shows the picture of a generalized gimbal, establishing the connection.

We present the study of head movement using two control strategies, *potential* and *optimal* control. The potential control strategy assumes that the muscles actuating the head movement are guided by an 'artificial' potential function, the minimum of which is adjusted by the final orientation of the specific head movement maneuver. Likewise, the optimal control strategy assumes that the three generalized torques on the model of the head are chosen to minimize a suitably defined quadratic cost function.²

² The control variables are the torques that are assumed to be unconstrained. In practice, these torque commands are generated by neck muscles that are not considered here.

Using the Tait–Bryan parametrization we simulate head movement trajectories using a new form of potential control, the main idea of which has already been introduced by Ghosh and Wijayasinghe (2012). We also augment the associated Euler Lagrange's equation (see Fox, 2010) by adding an appropriate damping term, and the simulated head movements are compared with recorded head movement data. The main purpose of this exercise is to ascertain the control strategy employed by the brain during head movements. *Do we move our heads, driven potentially or optimally?* In this paper, we try to answer this question by looking at the 'motion pathways' and the 'control signals' that generate these paths.

A model of the head movement dynamics is introduced, satisfying Donders' constraint. This step is similar to what was done in Ghosh and Wijayasinghe (2012), except that a new Tait–Bryan parametrization is considered and a new potential and damping term is chosen. Our potential control strategy repeats the essential steps in Ghosh and Wijayasinghe (2012), but we solve the optimal control problem using pseudospectral methods that are new to the head movement literature.

Human head movement dynamics, described later in this paper, is nonlinear and six dimensional. The associated optimal control problem is exceedingly difficult to solve analytically, and we implement a pseudospectral method to transform this optimal control problem into a nonlinear programming problem. This choice of discretization has many advantages (see Fahroo & Ross, 2001 and Stefanatos, Ruths, & Li, 2010). As a spectral method using orthogonal functions, the order of approximation (discretization) necessary to capture the dynamics is significantly smaller than conventional finite differences or Runge–Kutta techniques. As a direct collocation method, we can include arbitrary constraints and bounds to restrict both the controls and trajectories of the system. We use this ability to formulate the dynamics on $SO(3)$ and add a separate constraint to impose Donders' surface.

The paper enhances our ongoing study of constructing dynamic models for eye movement Polpitiya, Dayawansa, Martin, and Ghosh (2007) and head movement Ghosh and Wijayasinghe (2012). Earlier, we had used the axis angle parameters (using θ , ϕ and α) to describe these dynamics. Although axis angles are quite

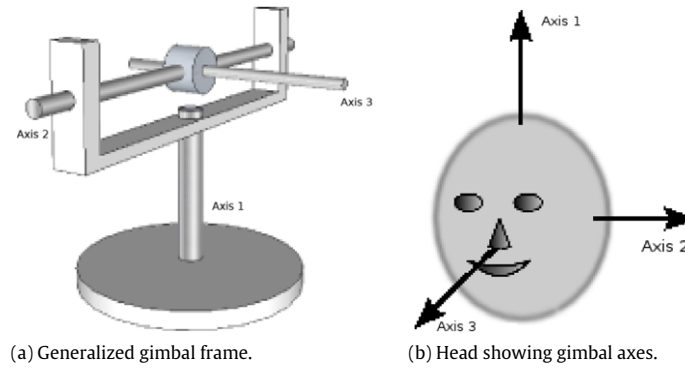


Fig. 2. Tait–Bryan angles are ϕ_1, ϕ_2, ϕ_3 where ϕ_i is counterclockwise head rotation, with respect to Axis i .

suitable for the purpose, the associated dynamical system on the space of orientations satisfying Listing’s constraint has a singularity along the frontal gaze direction. The Tait–Bryan parametrization (using ϕ_1, ϕ_2 and ϕ_3), proposed here, is better suited in terms of locations of the associated singularities.³ Using a suitable form of potential function and a damping term, the paper introduces a new dynamic model. Choice of this model is natural in the sense that even when a different coordinate system is chosen, the structure of the dynamical system is unaltered. Using this proposed dynamic model for head movement, we drive the head from an initial to a final orientation and compare simulated trajectories (using potential and optimal control) with experimentally recorded data from six human subjects. Such comparisons, we claim, are new in the literature.

Use of a nonlinear dynamic model enriches our simulations beyond what has been studied in Neuroscience Angelaki (2004), Tweed, Haslwanter, and Fetter (1998) and Tweed and vilis (1987) wherein no systematic comparison between observed and simulated trajectories is ever made. Significance of this paper is in the use of a dynamic model arising from classical mechanics Abraham and Marsden (1978) and Bullo and Lewis (2004). Earlier studies that had used dynamical systems are linear second order systems Kardamakis (2009), that ignore the manifold structure of the underlying space. We would like to speculate that models of the type proposed here can be applied in ‘Biomimetic control of a robotic head’ satisfying Donders’ constraints Cannata and Maggiali (2008).

2. Donders’ surface described by the Fick gimbal

Since every head orientation can be viewed as a point in $SO(3)$, head movements can be described as trajectories in $SO(3)$, the space of rotations. Parametrization of points in $SO(3)$ can easily be obtained from a parametrization of S^3 , the unit sphere in \mathbb{R}^4 . As described in Polpitiya et al. (2007), let us assume that the points in S^3 are unit quaternions with a coordinate map⁴ given by:

$$\rho : [0, 2\pi] \times [0, \pi] \times \left[-\frac{\pi}{2}, \frac{\pi}{2}\right] \rightarrow S^3 \quad (1)$$

where

$$\rho(\theta, \phi, \alpha) = \left(\cos \frac{\phi}{2}, \sin \frac{\phi}{2} \cos \theta \cos \alpha, \sin \frac{\phi}{2} \sin \theta \cos \alpha, \sin \frac{\phi}{2} \sin \alpha \right). \quad (2)$$

Next we consider the surjective 2 – 1 map *rot* from Polpitiya et al. (2007), between S^3 and $SO(3)$ given by

$$\text{rot} : S^3 \rightarrow SO(3). \quad (3)$$

The image of the composite map “ $\text{rot} \circ \rho(\theta, \phi, \alpha)$ ” is a rotation matrix which rotates a vector in \mathbb{R}^3 around the axis

$$(\cos \theta \cos \alpha, \sin \theta \cos \alpha, \sin \alpha)^T \quad (4)$$

by a counterclockwise angle ϕ . Note that when $\alpha = 0$, the axis (4) lies in a plane called Listing’s plane. It follows that α is the angle between the axis of rotation and Listing’s plane and θ is the angle between the projection of the axis of rotation on Listing’s plane and the positive x -axis (Axis 2 in Fig. 2).

Remark. The alpha parameters are not subsequently used in this paper except in describing the coordinate map ρ .

Going back to the Fick strategy for head movements, we can represent the horizontal rotation about the fixed vertical axis, by the quaternion

$$\rho_1 = \rho \left(\frac{\pi}{2}, \phi_1, 0 \right).$$

We can also represent the vertical rotation about the nested horizontal axis, by the quaternion

$$\rho_2 = \rho (0, \phi_2, \phi_1).$$

The resultant quaternion ρ_{fick} is obtained as a quaternion product (see Altmann, 2005) $\rho_{\text{fick}} = \rho_2 * \rho_1$ given by

$$\rho_{\text{fick}}(\phi_1, \phi_2) = \left(\cos \frac{\phi_1}{2} \cos \frac{\phi_2}{2}, \cos \frac{\phi_1}{2} \sin \frac{\phi_2}{2}, \sin \frac{\phi_1}{2} \cos \frac{\phi_2}{2}, -\sin \frac{\phi_1}{2} \sin \frac{\phi_2}{2} \right). \quad (5)$$

The two parameter families of quaternions (5) parameterize the set of all rotation matrices allowed by Fick Gimbals. If we denote

$$\rho_{\text{fick}}(\phi_1, \phi_2) = (q_0, q_1, q_2, q_3)^T \quad (6)$$

the Fick strategy implies that the q_i -s satisfy the relation

$$q_0 q_3 = -q_1 q_2, \quad (7)$$

and this Donders’ surface has already been introduced in the literature earlier (see for example Ceylan et al., 2000 and Glenn & Vilis, 1992). Note that in (5), two of the Tait–Bryan parameters have been introduced. In fact the roll angle ϕ_3 is assumed to be zero for Fick gimbals. In Section 4, this assumption is relaxed.

³ One can show that the singularities are located precisely when the gaze directions are ‘looking straight up’ or ‘looking straight down’.

⁴ Fick rotations are subsequently described using the coordinate map.

Table 1
For each of the 6 Donders' surfaces in Fig. 1, the parameters from Eq. (8) have been displayed.

| Data set | h_0 | $2h_1$ | $2h_2$ | h_{11} | h_{22} | $2h_{12}$ |
|----------|---------|---------|---------|----------|----------|-----------|
| 2 | -0.0087 | -0.0611 | +0.0628 | -0.1434 | -0.0067 | -2.2738 |
| 3 | -0.0129 | -0.0680 | -0.1032 | +0.1626 | -0.0015 | -0.2548 |
| 4 | +0.0036 | +0.0274 | -0.0919 | +0.2691 | +0.1695 | -0.4636 |
| 6 | -0.0010 | -0.0201 | +0.0148 | +0.0151 | -0.1667 | -2.5346 |
| 8 | -0.0062 | -0.0912 | +0.2553 | -0.4585 | -0.1278 | -1.0661 |
| 13 | +0.0094 | -0.0312 | +0.0262 | +0.5694 | +0.1996 | -2.4467 |

3. Donders' surfaces from human head movement data

We now briefly describe an experimental procedure to collect human head movement data recorded in conjunction with eye movement. For complete details on these experiments, we would refer to Glasauer, Hoshi, Kempermann, Eggert, and Büttner (2003) and Kremmyda, Glasauer, Guerrasio, and Büttner (2011). Data was recorded from 6 subjects,⁵ aged 25–38 years with no known neurological or orthopedic disorders. For 3D eye movement recordings, a dual search coil was used on the left eye (Skalar, Delft, The Netherlands) and for the 3D head movements, two coils mounted on a head ring at 90° angle between them was used. Both head and eye coils measured absolute position in the space. Therefore, when the head was allowed to move, the eye coil recorded gaze (combined eye and head) movements. When the head was fixed, gaze and eye movements were identical. Signals were sampled at 1 kHz. The subjects were seated in complete darkness inside a magnetic field (Remmel Labs) and were instructed to follow a laser dot (size 0.1°, distance 145 cm). Details on the calibration method are given elsewhere (Glasauer et al., 2003). Subjects had to follow the target with a combination of natural eye and head (gaze) movements. The laser dot jumped randomly between the center and eight peripheral positions by 28°, so that each final position is reached from a different initial position four times (maximum target jump is 56° horizontally and vertically). In each position the dot was first visible for 1000 ms, and then disappeared for 2500 ms and appeared again in the same position.

The head movement data had been recorded as a temporal sequence of orientation points, each point represented as a unit quaternion. A second order Donders' surface is obtained by least squares regression⁶ using the data points. We obtain six Donders' surfaces (sketched in Fig. 1) of the form

$$\bar{q}_3 = h_0 + 2h_1\bar{q}_1 + 2h_2\bar{q}_2 + h_{11}\bar{q}_1^2 + h_{22}\bar{q}_2^2 + 2h_{12}\bar{q}_1\bar{q}_2, \quad (8)$$

whose parameters are displayed in Table 1. In (8) the scaled coordinates \bar{q}_i are defined as $\bar{q}_i = \frac{q_i}{q_0}$, for $i = 1, 2, 3$.

4. Tait–Bryan parametrization of Donders' surface

In this section, we introduce the Tait–Bryan angles (Dunn & Parberry, 2011; O'Reilly, 2008), given by ϕ_1, ϕ_2, ϕ_3 that generalize the gimbal coordinates introduced in Section 2. The first two angles are defined as before (see Sections 1 and 2) for the Fick gimbal. An additional third angle ϕ_3 measures rotation with respect to a third axis which is initially orthogonal to the first two axes of head

rotation. The instantaneous direction of this third axis is obtained by rotating it by ϕ_1 with respect to the first axis and by ϕ_2 with respect to the rotated second axis. Analogous to (5), it turns out that the resultant quaternion is given by

$$\rho_{\text{Tair}}(\phi_1, \phi_2, \phi_3) = \begin{pmatrix} \sin \frac{\phi_1}{2} \sin \frac{\phi_2}{2} \sin \frac{\phi_3}{2} + \cos \frac{\phi_1}{2} \cos \frac{\phi_2}{2} \cos \frac{\phi_3}{2} \\ \cos \frac{\phi_1}{2} \sin \frac{\phi_2}{2} \cos \frac{\phi_3}{2} + \sin \frac{\phi_1}{2} \cos \frac{\phi_2}{2} \sin \frac{\phi_3}{2} \\ \sin \frac{\phi_1}{2} \cos \frac{\phi_2}{2} \cos \frac{\phi_3}{2} - \cos \frac{\phi_1}{2} \sin \frac{\phi_2}{2} \sin \frac{\phi_3}{2} \\ \cos \frac{\phi_1}{2} \cos \frac{\phi_2}{2} \sin \frac{\phi_3}{2} - \sin \frac{\phi_1}{2} \sin \frac{\phi_2}{2} \cos \frac{\phi_3}{2} \end{pmatrix}. \quad (9)$$

In the above representation, $\phi_3 = 0$ reduces to (5), the quaternion obtained from Fick gimbals. In general, ϕ_3 is assumed to be nonzero and we impose Donders' constraint by restricting ϕ_3 as a function of ϕ_1 and ϕ_2 in (9).⁷

We now normalize the above quaternion (9) by dividing each term by $\cos \frac{\phi_3}{2}$ and substitute the coordinates in Donders' surface (8). This way, we obtain a quadratic equation in $\tan \frac{\phi_3}{2}$ given by

$$t \tan^2 \frac{\phi_3}{2} + s \tan \frac{\phi_3}{2} + r = 0, \quad (10)$$

where t, s and r are functions of ϕ_1 and ϕ_2 , details of which are in the Appendix. For those angle variables ϕ_1, ϕ_2 for which $s^2 - 4tr \geq 0$, we solve ϕ_3 as a function of ϕ_1 and ϕ_2 .

When the discriminant is strictly positive, one can solve (10) for ϕ_3 up to two distinct choices. Since specifying the angles ϕ_1 and ϕ_2 completely specifies the head-pointing direction of the head given by

$$\rho_1 = (\sin \phi_1 \cos \phi_2 \quad -\sin \phi_2 \quad \cos \phi_1 \cos \phi_2)^T \quad (11)$$

the two choices of ϕ_3 for a given head-pointing direction would correspond to two distinct orientations.

5. Head movement dynamics with a potential function and damping

Our goal in this section is to write down a dynamical system for head movement using the Tait–Bryan parametrization introduced in Section 4. This is done by introducing an appropriate Lagrangian formulation, the main ideas of which are already sketched in Ghosh and Wijayasinghe (2012) and Polpitiya et al. (2007). For the purpose of setting up the notation, we rewrite the main steps as follows.

Let $q(\phi_1, \phi_2)$ be a parametrization,⁸ of points in S^3 that satisfy Donders' constraint (10).⁹ We label this space by *DOND* and define

$$G = \begin{pmatrix} q_{\phi_1} \cdot q_{\phi_1} & q_{\phi_1} \cdot q_{\phi_2} \\ q_{\phi_2} \cdot q_{\phi_1} & q_{\phi_2} \cdot q_{\phi_2} \end{pmatrix}, \quad (12)$$

where $q_\gamma = \frac{\partial q}{\partial \gamma}$ and where γ is either ϕ_1 or ϕ_2 . Let $X = (\phi_1, \phi_2)^T$ be the vector of angle variables. As in Polpitiya et al. (2007), we would define the kinetic energy¹⁰ *KE* as

$$KE = \frac{1}{2} \dot{X}^T G \dot{X}. \quad (13)$$

⁷ Note that a nonzero ϕ_3 corresponds to a nonzero roll.

⁸ We obtain this parametrization from (9) by writing ϕ_3 as a function of ϕ_1 and ϕ_2 given by (10).

⁹ As evident from Fig. 1, choice of Donders' constraint would differ from subject to subject, and this would lead to subject wise variation in the head movement dynamics.

¹⁰ The head is assumed to be a perfect sphere with mass distributed uniformly. The rotation is assumed to be about the center of the sphere.

⁵ Six subjects are chosen out of a total of 13 subjects recorded, leading up to six choices of Donders' surfaces in Fig. 1. The numbering on the surface refers to this data set. The choice of the surfaces is randomly picked examples and there is no particular significance in choosing 6 surfaces.

⁶ A system of linear equation is written on the coefficient space of (8) using the recorded data \bar{q}_i . The coefficients are now calculated using matrix pseudoinverse (Campbell & Meyer, 1991).

If the potential energy is represented by V , the Lagrangian of the head movement system can be written as

$$L = KE - V. \quad (14)$$

The equation of motion on *DOND* using the Euler Lagrange equation can now be described as

$$\frac{d}{dt} \frac{\partial L}{\partial \dot{\gamma}} - \frac{\partial L}{\partial \gamma} = \tau_\gamma \quad (15)$$

where γ is defined as before and where τ_γ is the generalized torque input to the system. The resulting equations of motion can be expressed as

$$G\ddot{X} + \dot{G}\dot{X} - \nabla_X L = \Gamma, \quad (16)$$

where $\Gamma = (\tau_{\phi_1} \quad \tau_{\phi_2})^T$ and where ∇_X is the gradient operator with respect to X defined as

$$\nabla_X = \left(\frac{\partial}{\partial \phi_1}, \frac{\partial}{\partial \phi_2} \right)^T. \quad (17)$$

5.1. Choice of a potential function

Potential functions are added to the Lagrangian (14) so that the head movement trajectory can move toward points of least potential. The potential function we consider in this paper is described as follows

$$V(\phi_1, \phi_2) = A (1 - |q(\phi_1, \phi_2) \cdot q_0|) \quad (18)$$

where q_0 is a fixed unit quaternion on Donders' surface and $q(\phi_1, \phi_2) \cdot q_0$ represent the dot product of two vectors in \mathbb{R}^4 . It can be observed that the minima occur at $q = q_0$ or $q = -q_0$. Both of these minima correspond to a unique point on $SO(3)$ via the map "rot" introduced in (3).

It would follow that with the choice of the potential function (18), one can steer the head toward the orientation represented by $q = \pm q_0$. Note also that the description (18) of the potential function does not change for a different choice of coordinates.

5.2. Selection of a damping term

A damping term is added externally using the generalized torque input Γ , the goal of which is to dampen the movement of the head so that it quickly comes to a rest at the desired pointing direction and orientation. An earlier paper Ghosh and Wijayasinghe (2012) had considered the following form of damping:

$$\Gamma = -K \dot{X},$$

where $K = \text{diag}(k_1 \quad k_2)$. This choice of the damping term is coordinate dependent and we modify the choice of damping to the following form:

$$\Gamma = -c G \dot{X}, \quad (19)$$

where c is an arbitrary constant and G is the matrix defined in (12). With the choice of damping (19), the EL equation (16) reduces to

$$G \ddot{X} + (\dot{G} + cG) \dot{X} = \nabla_X L. \quad (20)$$

6. Head movement as a potential control problem

Consider the head movement dynamics on *DOND*, described by the EL equation (20). The potential function (18) drives the state of the head from an initial to a final orientation. One can separate

the contribution of the potential and the damping term and rewrite (20) as

$$G\ddot{X} + \dot{G}\dot{X} - \frac{1}{2} \dot{X}^T \nabla_X G \dot{X} = \tilde{F} \quad (21)$$

where we write \tilde{F} as

$$\tilde{F} = -\nabla_X V - c G \dot{X}. \quad (22)$$

The head movement dynamical system can now be viewed as being controlled by \tilde{F} where the contributions of the potential and the damping terms can be implemented by a controller. If the goal is to drive the head to a suitable final orientation, one can choose an appropriate q_0 in (18) and implement the controller (22). This, in essence, is the *potential control problem*. We now propose to extend the potential control formulation (21), (22) as a dynamical system on S^3 (instead of *DOND*). Donders' constraint is additionally imposed using the Lagrange multiplier. The details are described as follows.

Let $q(\phi_1, \phi_2, \phi_3)$ be a parametrization of points in S^3 given by (9). We define a Riemannian metric on S^3 computed from a 3×3 matrix G , analogous to (12), where $q_\gamma = \frac{\partial q}{\partial \gamma}$. Let $X = (\phi_1, \phi_2, \phi_3)^T$ be the vector of angle variables. As in Polpitiya et al. (2007), we would define the kinetic energy KE as

$$KE = \frac{1}{2} \dot{X}^T G \dot{X}. \quad (23)$$

As in (18), if the potential energy V is chosen as

$$V(\phi_1, \phi_2, \phi_3) = A (1 - |q(\phi_1, \phi_2, \phi_3) \cdot q_0|), \quad (24)$$

where q_0 is a fixed unit quaternion in *DOND* and $q(\phi_1, \phi_2, \phi_3) \cdot q_0$ represent the dot product of two vectors in \mathbb{R}^4 , the Lagrangian of the head movement system can be written as

$$L = KE - V. \quad (25)$$

We can impose Donders' constraint at this point by defining

$$\tilde{L} = L + \lambda F = KE - V + \lambda F, \quad (26)$$

where $F \equiv 0$ is Donders' constraint (of the kind described in (10)) and λ is the Lagrange multiplier. The equations of motion in S^3 subjected to Donders' constraint can then be derived by using the Euler Lagrange equations which can be described as

$$\frac{d}{dt} \frac{\partial \tilde{L}}{\partial \dot{\gamma}} - \frac{\partial \tilde{L}}{\partial \gamma} = \tau_\gamma, \quad (27)$$

where γ is the angle variables ϕ_1, ϕ_2, ϕ_3 and λ , and where τ_γ is the generalized torque input to the system and $\tau_\lambda = 0$. The resulting equations of motion can be expressed as

$$G\ddot{X} + \dot{G}\dot{X} - \frac{1}{2} \dot{X}^T \nabla_X G \dot{X} + \nabla_X V - \lambda \nabla_X F = \Gamma, \quad (28)$$

where $\Gamma = (\tau_{\phi_1}, \tau_{\phi_2}, \tau_{\phi_3})^T$ and ∇_X is the gradient operator with respect to X . The definition of the gradient operator is similar to (17). Eq. (28) can be written in a reduced form as

$$G\ddot{X} + \dot{G}\dot{X} - \nabla_X \tilde{L} = \Gamma. \quad (29)$$

As in Section 5.2, we would add a damping term of the form (19) and write (29) as (21), where we define a new torque \tilde{F} as

$$\tilde{F} = \lambda \nabla_X F - \nabla_X V - c G \dot{X}. \quad (30)$$

The system of Eqs. (21), (30) (where the state variable $X = (\phi_1, \phi_2, \phi_3)^T$), together with Donders' constraint $F \equiv 0$ provides a description of a potentially controlled dynamical system for which the Lagrange multiplier $\lambda(t)$ can be computed implicitly.¹¹

¹¹ The potential control approach introduced shares the same framework with equilibrium point hypothesis (EPH), used by a lot of researchers in human motor control (see for example Feldman & Latash, 2005 and Gomi & Kawato, 1996).

7. Optimal control using the pseudospectral method

In this section, we reconsider the head movement dynamics (21), without the assumption that the control \tilde{T} is generated from (30), using a potential function V , a damping term together with a Lagrange multiplier. These terms are assumed to be absent from the head movement dynamics and the control \tilde{T} is written as $(\tau_{\phi_1}, \tau_{\phi_2}, \tau_{\phi_3})^T$. As before, the state vector X is given by $(\phi_1, \phi_2, \phi_3)^T$.

For a given T , the optimal control problem we propose to consider is to drive the state (X, \dot{X}) from a given initial value $(X(0), 0)$ to a given final value $(X(T), 0)$ while minimizing the cost function

$$\int_0^T [\tau_{\phi_1}^2(t) + \tau_{\phi_2}^2(t) + \tau_{\phi_3}^2(t)] dt. \quad (31)$$

The initial and the final values of the state are assumed to lie on Donders' surface (10) and the control torques are computed so that the states evolve on this Donders' surface as well.¹²

The absence of the damping term is justified by the fact that, in the optimal control framework, an undamped response is observed in simulation to be more costly compared to a damped response. The absence of the potential term is justified by the fact that the constraint on the final state is a part of the optimal control formulation, and hence does not have to be separately imposed using a potential function.

Redefining the state variables as $\xi_1 = (\phi_1, \phi_2, \phi_3)^T$ and $\xi_2 = (\dot{\phi}_1, \dot{\phi}_2, \dot{\phi}_3)^T$, the EL equation (28) is written as

$$\dot{\xi}_1 = \xi_2; \quad G \dot{\xi}_2 + \dot{G} \xi_2 - \frac{1}{2} \xi_2^T \nabla_{\xi_1} G \xi_2 = \tau_{\phi}. \quad (32)$$

Donders' constraint (10) is given by $F(\xi_1) = 0$, where

$$F(\xi_1) = t(\phi_1, \phi_2) \tan^2 \frac{\phi_3}{2} + s(\phi_1, \phi_2) \tan \frac{\phi_3}{2} + r(\phi_1, \phi_2),$$

and t, s, r are defined in the Appendix. The boundary conditions are given by

$$\xi_1(0) = (\phi_{10}, \phi_{20}, *), \quad \xi_1(T) = (\phi_{1T}, \phi_{2T}, *), \\ \xi_1(0) = \dot{\xi}_1(T) = (0, 0, 0), \quad \forall t \in [0, T].$$

The control τ_{ϕ} is described by the vector $(\tau_{\phi_1}, \tau_{\phi_2}, \tau_{\phi_3})$ of generalized torques and $*$ denotes a free parameter so that the initial and final states lie on Donders' surface (10).

Taken together, the preceding cost function (31), dynamics (32), and Donders' state-constraint (10) form an optimal control problem. While analytical methods (i.e., the maximum principle) exist to solve such problems, systems of this size and complexity are typically intractable and, therefore, require computational methods to solve them (Pontryagin, Boltyanskii, Gamkrelidze, & Mishchenko, 1962). A variety of numerical methods exist for solving optimal control problems and can generally be classified as either direct or indirect. An indirect method finds approximate solutions to the two point boundary value problem given by the necessary conditions of the maximum principle. Applying an indirect method requires first solving for this set of coupled state and adjoint equations. When working with complex nonlinear systems, especially those employing nonlinear constraints, this can be both difficult and tedious. A direct method avoids these issues by directly discretizing the original problem into a nonlinear programming problem. Since all variables are physically relevant

to the problem (contrast this with adjoint variables in indirect methods), this facilitates adding additional constraints as needed. For these reasons, we use a direct method to solve for the optimal torques.

We implement a pseudospectral method to solve the optimal control problem described above. This method relies on approximation by orthogonal polynomials (in our case we use the Legendre polynomials), which admits spectral accuracy, similar to a Fourier approximation for periodic functions (Boyd, 2000). This type of approach has been used effectively to solve problems in fluid dynamics, and since then the related concepts have been successfully applied in a wide variety of domains, including satellite motion (Fahroo & Ross, 2001) and quantum mechanics (Stefanatos et al., 2010). The pseudospectral method uses orthogonal polynomial expansion to approximate the states and controls of the system and thereby inherit the spectral accuracy characteristic of such expansions (Ruths & Li, 2011) (the k th coefficient of the expansion decreases faster than any inverse power of k Canuto, Hussaini, Quarteroni, & Zang, 2006). Using recursive properties unique to certain classes of orthogonal polynomials, e.g. Legendre and Chebyshev, derivatives of the states can again be expressed in terms of the orthogonal polynomial expansions, making it possible to accurately approximate the differential equation that describes the dynamics with an algebraic relation imposed at a small number of discretization points.

The pseudospectral method discretizes the continuous cost, dynamics, and constraints using interpolation on a set of Gauss–Lobatto nodes specially selected for near-optimal convergence in terms of the approximation (Smith, 2006). Using an expression that relates the $k+1$ and k terms of the interpolation functions, we can rewrite the dynamics as an algebraic relation. Leveraging the interpolation on the selected nodes in a different way permits a highly accurate approximation of the integrated cost, using the Gaussian quadrature (Canuto et al., 2006). For additional details on the computational method, see Boyd (2000).

8. Results

An important result of this paper is displayed in the form of trajectories sketched in Figs. 3 and 4 using scaled coordinates $\bar{q}_i = \frac{q_i}{q_0}$ for $i = 1, 2, 3$ (see Eq. (6)). For each of the six subjects, from which the head movement data has been collected, the figures display how the trajectories generated by the potential and the optimal controller compare with the recorded head movement data.¹³

For each of the six subjects, multiple trajectories have been picked and the corresponding trajectories are displayed in Fig. 4, together with the simulated potential and optimal trajectories. Out of the multitude of trajectories, one specific trajectory has been picked for each of the six subjects and displayed in Fig. 3. For ease of display, in Fig. 4 we have used only two of the three scaled coordinates \bar{q}_1, \bar{q}_2 . Ideally, since the head orientations satisfy Donders' constraint (8), it would follow that \bar{q}_3 depends completely on \bar{q}_1 and \bar{q}_2 .

The optimal control torques and trajectories are obtained over a fixed duration $T = 1$ with initial and final conditions for (ϕ_1, ϕ_2) taken from recorded head movement trajectories. The optimal controller is computed ensuring that the state remains sufficiently close to Donders' surface. For the purpose of comparison, the parameters in the potential control are adjusted so that the final time is approximately $T = 1$. This is achieved by choosing the potential

¹² We remark that Donders' constraint is implemented directly, while solving the optimal control problem numerically, and not with the aid of Lagrange's multiplier, as has been the case in (26). The Lagrange multiplier is assumed to be 0.

¹³ Recall that, during data collection, the human subjects directly moved their head between two pointing directions.

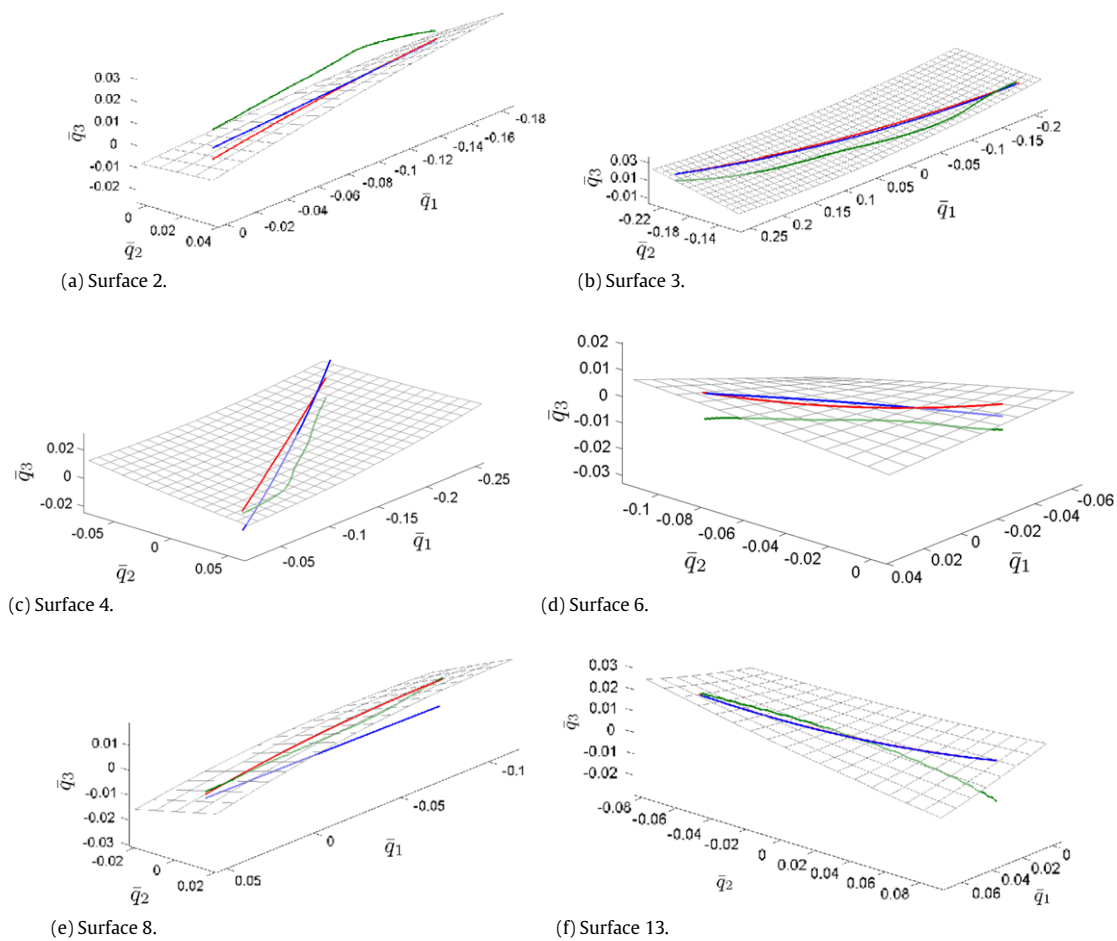


Fig. 3. One specific head movement trajectory is shown for each of the six Donders' surfaces in Fig. 1 on the coordinate space \bar{q}_1 , \bar{q}_2 and \bar{q}_3 . The surface indices are indicated above. Green lines are from the experimentally collected head movement data. Red lines are from the simulated trajectories using potential control (29), (30), where V is described in (24). Blue lines are from the simulated trajectories using optimal control minimizing (31). Parameters A and c are chosen as 35 and 10, respectively.

control coefficient A in (24) to be 35 and the friction coefficient c in (19) to be 10.

We calculated the maximum error percentage between the simulated and the recorded trajectories for each of the trajectories in Fig. 4. The error is computed as an angle between the corresponding unit quaternion vectors after we have reparameterized each point of a trajectory as a function of the arc length. Finally, the error is obtained as a percentage of the angle between the initial and final unit quaternion vectors. From these errors obtained, we observed that the percentage of maximum error between simulated and recorded trajectories vary, roughly between 3% and 23%, where the percentage is calculated with respect to the total angular deviation between the initial and final points of the trajectory.¹⁴ By and large, the maximum error is observed to be less than 2°.

For each of the six cases displayed in Fig. 3, the potential and the optimal control torques are displayed in Figs. 5 and 6. The three components of the torques are displayed in three different colors. The costs of potential and optimal controls are computed, using (31), for each of the six subjects undergoing ten different head movement maneuvers, shown in Fig. 4. These results, displayed in Fig. 7 show that by and large the cost of potential control is about five times more than the cost of optimal control.

¹⁴ Note that while calculating the errors, the temporal dependence of the trajectories is not looked into. Also higher percentage errors are for shorter trajectories.

9. Discussions

On viewing the controllers sketched in Figs. 5, 6 we observe that the potential controller takes a relatively large value during the initial phase of the control action. The magnitude of the control tapers off subsequently, receding to the value 0 at the final time $T = 1$. The optimal controller, on the other hand, remains relatively active throughout the time interval $[0, 1]$ and does not approach 0 at the final time. In practice this would imply that the optimal controller has a discontinuity at $T = 1$. In view of its structure, we comment that the potential controller mimics a PD (proportional–derivative) controller (Ang, Chong, & Yun, 2005).

The simulated trajectories arising from potential and optimal controllers differ from the corresponding trajectories recorded from the head movement data in essentially two ways. First of all, the simulated trajectories are closely restricted to the constraint imposed by Donders, whereas the recorded trajectories are not entirely restricted by Donders' surface, i.e., there are small deviations away from the surface. This is evident in Fig. 3. Second, restricted to Donders' surface, the simulated data differs from the recorded data essentially by virtue of the fact that simulated head movements do not allow for 'excursions' during the transition between initial and final orientations. This is evident when the trajectories are projected on the (\bar{q}_1, \bar{q}_2) plane (see Fig. 4, where the simulated trajectories are 'almost linear' whereas the recorded trajectories do have some amount of curvature). The curvature may have been introduced artificially when the recorded movement data was split up into a cascade of trajectories, with initial and

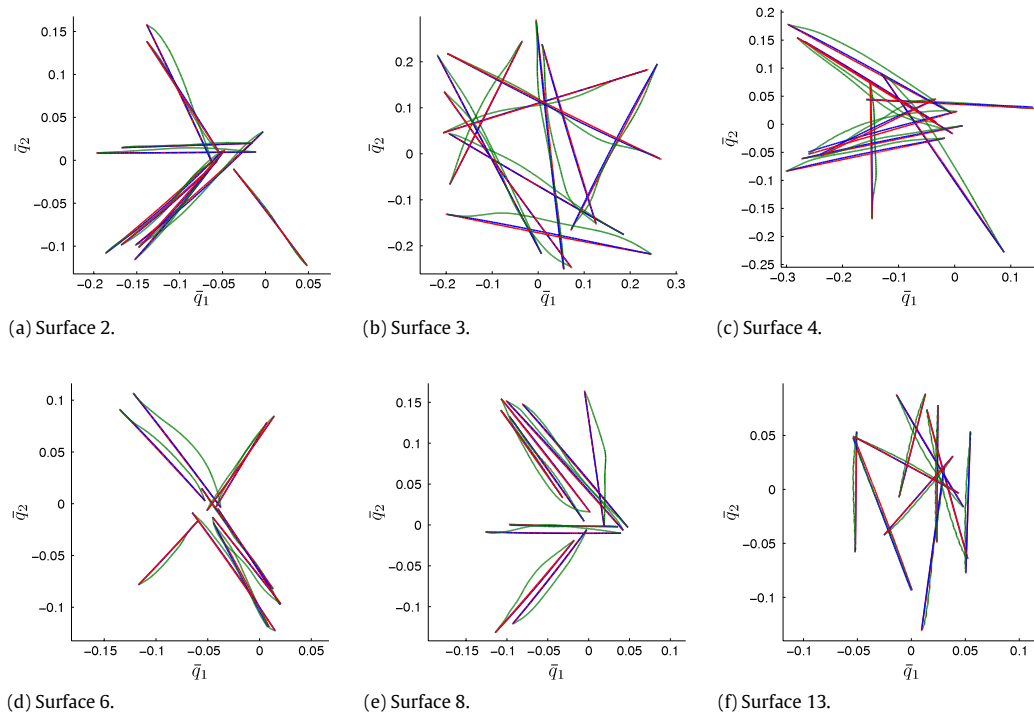


Fig. 4. Head movement trajectories are shown for six surfaces in Fig. 1. Green lines are the trajectories from the experimentally collected head movement data. Red lines are the head movement trajectories using potential control with parameters chosen as in Fig. 3. Blue lines are the head movement trajectories generated using optimal control minimizing (31). All trajectories are displayed by projecting on to the $\bar{q}_1\bar{q}_2$ plane where $\bar{q}_1 = \frac{q_1}{q_0}$ and $\bar{q}_2 = \frac{q_2}{q_0}$.

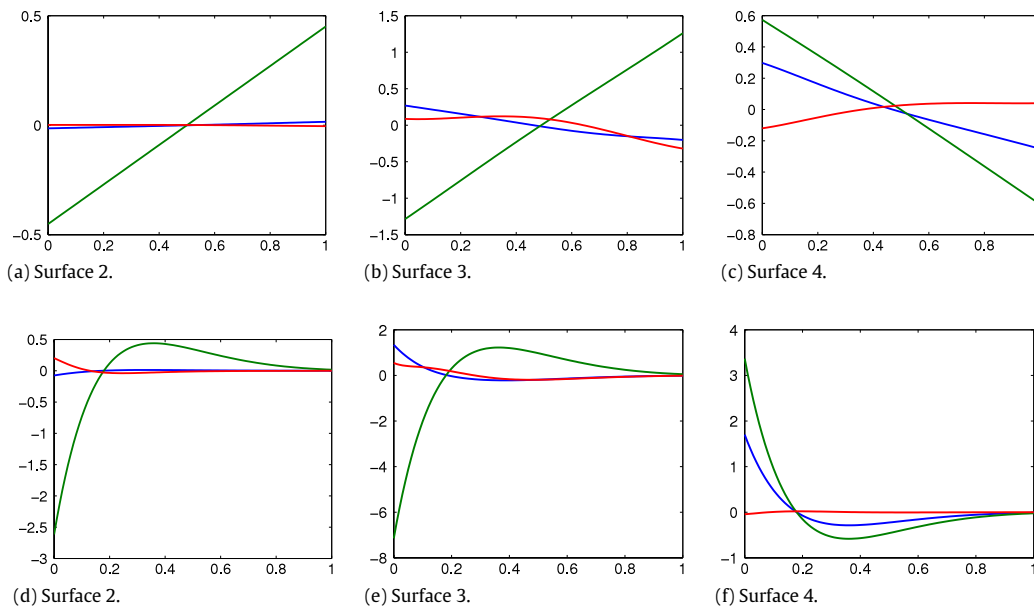


Fig. 5. Comparison of torques from the optimal control vs. torques from the potential control for Donders' surfaces 2, 3 and 4. Blue is τ_{ϕ_1} , Green is τ_{ϕ_2} and Red is τ_{ϕ_3} . Top figures, left to right are optimal torques from Fig. 3(a)–(c). Bottom figures, left to right are potential torques from Fig. 3(a)–(c).

final pointing directions recognized when the head is observed to stop momentarily. The curvature may be a result of the subject hesitating, before settling on a final head pointing direction. The potential or the optimal trajectories do not capture these effects.¹⁵

¹⁵ The observed difference between the simulated and the experimentally observed trajectories may be due to dynamic factors affecting Donders' surface. Unfortunately, this fact could not be verified because our data is not rich enough to capture the dynamics of the surface, if any.

In the head movement experiments that generated the data, the generalized torques applied to the head are not directly measured. Hence it is not possible to compare the actual cost of control with the cost of controls recorded in Fig. 7. It is however possible to estimate the generalized torques τ_{ϕ_1} , τ_{ϕ_2} , τ_{ϕ_3} , using the recorded trajectories of the head orientations and the model (32). For the trajectories displayed as green lines in Fig. 3, the generalized torques are computed and plotted in Fig. 8. One should compare the estimates of the generalized torques in Fig. 8 with the torques

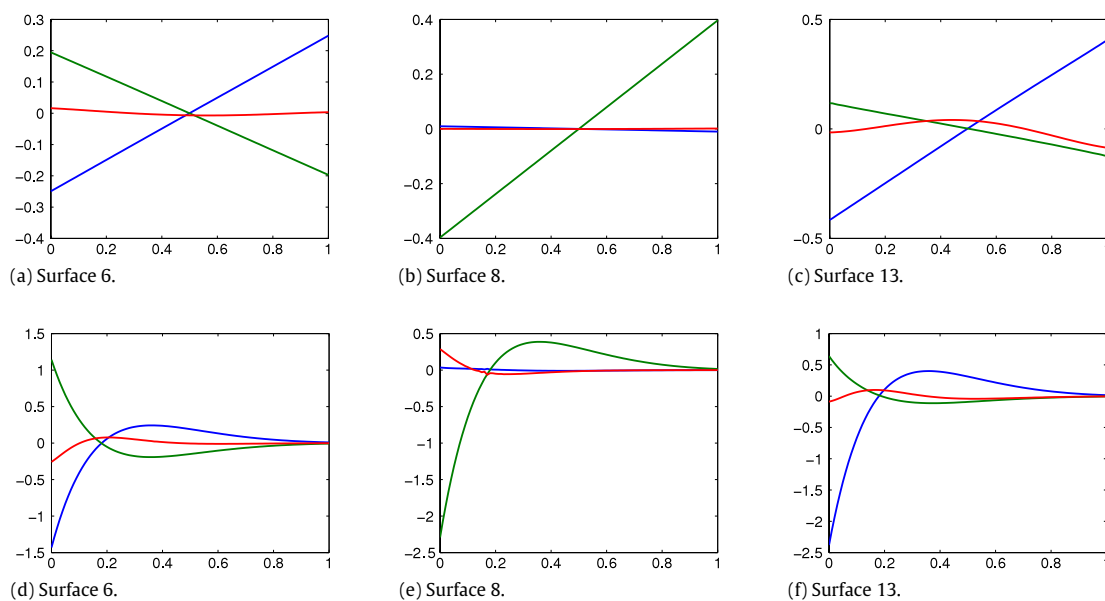


Fig. 6. Comparison of torques from the optimal control vs. torques from the potential control for Donders' surfaces 6, 8 and 13. Blue is τ_{ϕ_1} , Green is τ_{ϕ_2} and Red is τ_{ϕ_3} . Top figures, left to right are optimal torques from Fig. 3(d)–(f). Bottom figures left to right are potential torques from Fig. 3(d)–(f).

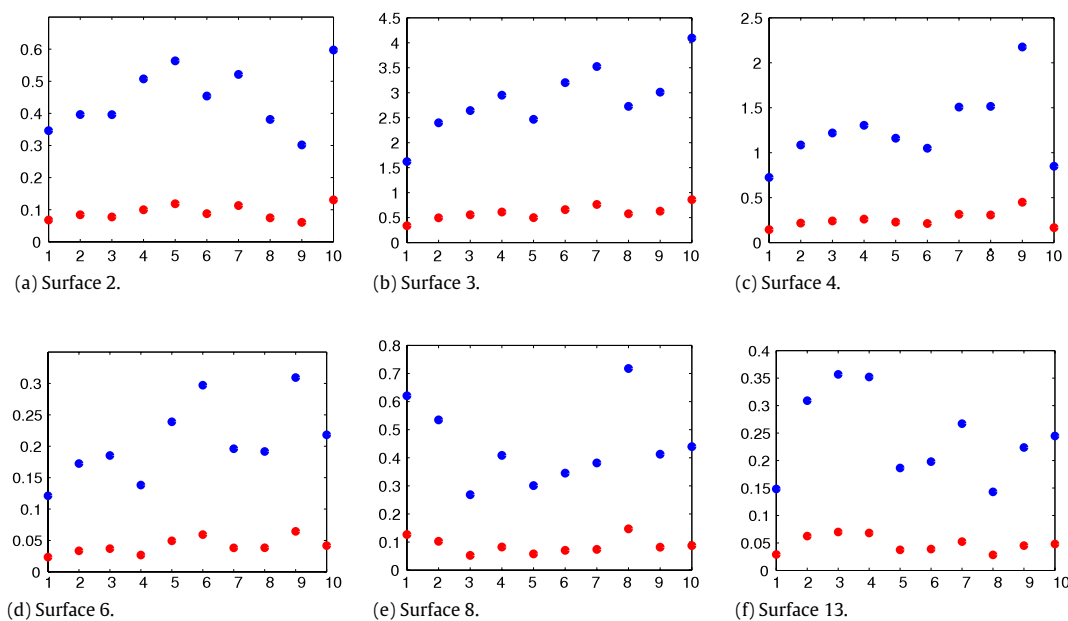


Fig. 7. Values of the cost function (31) for the potential and optimal control are plotted in the y-axis. In the x-axis we have the trajectory index for each of the 10 trajectories in Fig. 4. The optimal control has been plotted in red whereas the potential control is shown in blue.

obtained in Figs. 5, 6 for the potential and optimal control tasks. The following points are noted.

Qualitatively, the estimated torques (in Fig. 8) do not asymptotically approach zero,¹⁶ i.e., the controls remain active throughout the time interval as is the case with optimal torques and unlike the potential torques (in Figs. 5, 6). The costs of the estimated torques, measured by (31), show that their values are close to the optimal torques described in Fig. 7 (see Table 2). In some cases the cost of the estimated torques is less than what is computed for the optimal torques. This is possibly because the optimal control is derived for

Table 2

The table shows costs of estimated torques from Fig. 8. The trajectory numbers correspond to the indices displayed in Fig. 7. Only one trajectory out of ten has been chosen for each of the six surfaces, as displayed in Fig. 3.

| Surface # | 2 | 3 | 4 | 6 | 8 | 13 |
|----------------|--------|--------|--------|--------|--------|--------|
| Trajectory # | 1 | 8 | 1 | 2 | 3 | 2 |
| Cost from (31) | 0.0885 | 0.3481 | 0.0321 | 0.0184 | 0.0166 | 0.0210 |

a trajectory restricted entirely on Donders' surface, whereas the estimated torques are derived on a trajectory that often deviates out of Donders' surface (see Fig. 3).

None of the six subjects in this paper used potential based control as evident from the cost of the control signals, which

¹⁶ Although in some cases they were close to zero.

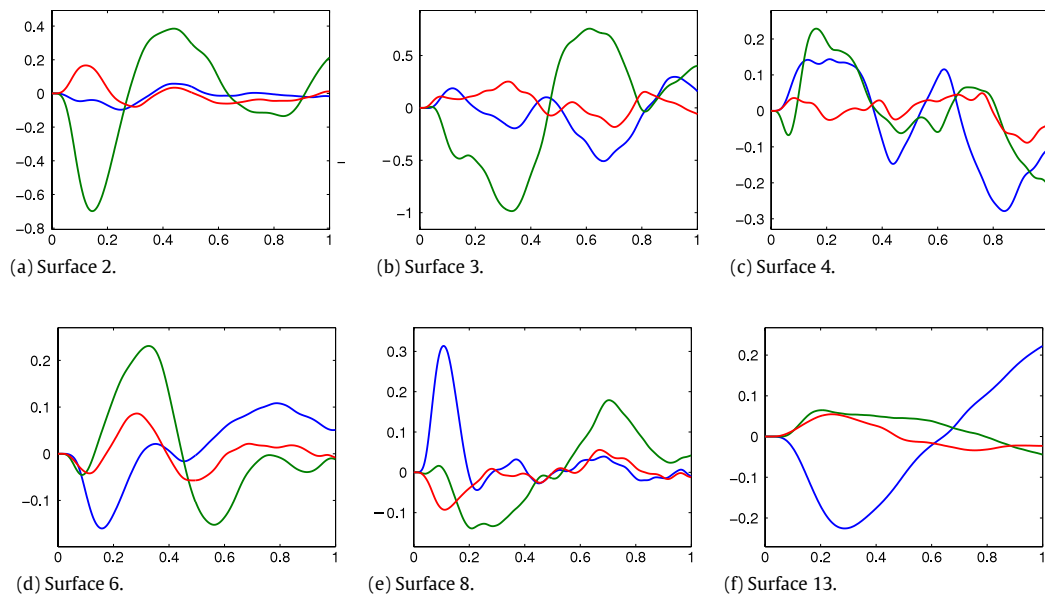


Fig. 8. Torques computed from recorded head movement data (displayed as green lines in Fig. 3), and the model (32). Blue is τ_{ϕ_1} , Green is τ_{ϕ_2} and Red is τ_{ϕ_3} .

was found to be close to that of the proposed optimal control. While subjects used a control that generated head movement trajectories close to both the potential and optimal trajectories, the estimated control functions differ not only from the predictions of potential control, but also from those of the optimal control. It is unclear (and a good question for future research) whether the differences between the estimated actual control strategy used by the subjects and the proposed optimal control are due to, for example, differences in head dynamics or cost function used.¹⁷

10. Conclusion

This paper introduces a dynamic model of human head rotation, using a newly introduced Tait–Bryan parametrization. The space of head orientations is viewed as a (Donders’) submanifold of unit quaternions, endowed with a Riemannian metric. The movement dynamics is derived by writing the associated Euler Lagrange’s equation, with a generalized torque as control. The control problem, we consider, is to drive the orientation vector from a given initial value to a given final value, staying within the Donders’ submanifold, while maintaining the time derivative to be zero at the two boundaries. Two different control strategies are introduced. In the *potential control* strategy, the orientation vector is driven by a gradually reducing potential function, attaining the zero value at the end point. In the *optimal control* strategy, the orientation vector is transferred between the two boundary points by a minimum energy controller. A direct, pseudo-spectral method is introduced to derive the optimal controller.

To highlight the main points of this paper, simulated trajectories using the model we propose closely capture experimentally observed head movements, except that transient excursions are not captured. Moreover, the cost of the estimated control, our subjects use, is close to the optimal cost. The paper is inconclusive about the strategy our brain uses to generate the control signals.

Acknowledgments

Any opinions, findings, and conclusions or recommendations expressed in this material are those of the author(s) and do not necessarily reflect the views of the National Science Foundation.

Appendix

In this section, we derive an explicit expression of t , s and r in (10) as follows. We choose the four coordinates q_0, q_1, q_2, q_3 , from (9) and substitute them in a modified form of (8) given by

$$\hat{q}_0 \hat{q}_3 = h_0 \hat{q}_0^2 + 2h_1 \hat{q}_0 \hat{q}_1 + 2h_2 \hat{q}_0 \hat{q}_2 + h_{11} \hat{q}_1^2 + h_{22} \hat{q}_2^2 + 2h_{12} \hat{q}_1 \hat{q}_2,$$

where $\hat{q}_i = \frac{q_i}{\cos \frac{\phi_3}{2}}$. The functions t , s and r can be readily read off as follows:

$$\begin{aligned} t &= h_{11} \cos^2 \left(\frac{\phi_2}{2} \right) \sin^2 \left(\frac{\phi_1}{2} \right) + \frac{1}{2} (h_0 + h_{22} \\ &\quad + (h_{22} - h_0) \cos(\phi_1) - 2h_2 \sin(\phi_1)) \sin^2 \left(\frac{\phi_2}{2} \right) \\ &\quad - \frac{1}{4} (2h_1 (\cos(\phi_1) - 1) + (2h_{12} + 1) \sin(\phi_1)) \sin(\phi_2), \\ s &= \frac{1}{2} ((2h_{12} - 1) \cos(\phi_2) - \cos(\phi_1) (2h_{12} + 2h_2 \sin(\phi_2) + 1)) \\ &\quad + \frac{1}{2} (\sin(\phi_1) (2h_1 + (h_0 + h_{11} - h_{22}) \sin(\phi_2))), \\ r &= \frac{1}{4} (h_0 + h_{11} + h_{22} + \cos(\phi_1) (h_0 + h_{11} - h_{22} \\ &\quad + (h_0 - h_{11} - h_{22}) \cos(\phi_2))) + \frac{1}{4} (2h_2 \sin(\phi_1) \\ &\quad + \cos(\phi_2) (h_0 - h_{11} + h_{22} + 2h_2 \sin(\phi_1))) \\ &\quad + \frac{1}{4} ((2h_1 (\cos(\phi_1) + 1) + (2h_{12} + 1) \sin(\phi_1)) \sin(\phi_2)). \end{aligned}$$

References

Abraham, R., & Marsden, J. E. (1978). *Foundations of mechanics*. Providence, Rhode Island: AMS Chelsea Publishing, American Mathematical Society.
 Altmann, S. L. (2005). *Rotations, quaternions, and double groups*. Oxford University Press (Hardcover), 1986. Dover Publications (Paperback).

¹⁷ One reason why the predicted torques in Figs. 5, 6 are different from the estimated torque in Fig. 8 is that in our analysis we were ignoring the temporal profile of the trajectories, concentrating entirely on the spatial variations.

- Ang, K. H., Chong, G., & Yun, L. (2005). PID control system analysis, design and technology. *IEEE Transactions on Control Systems Technology*, 13(4), 559–576.
- Angelaki, D. (2004). Eyes on target: what neurons must do for the vestibuloocular reflex during linear motion. *Journal of Neurophysiology*, 92, 20–35.
- Boyd, J. (2000). *Chebyshev and fourier spectral methods* (2nd ed.). New York: Dover Publications.
- Bullo, F., & Lewis, A. D. (2004). *Texts in applied mathematics: Vol. 49. Geometric control of mechanical systems*. New York, Heidelberg, Berlin: Springer Verlag.
- Campbell, S. L., Jr., & Meyer, C. D. (1991). *Generalized inverses of linear transformations*. New York: Dover.
- Cannata, G., & Maggiali, M. (2008). Models for the design of bioinspired robot eyes. *IEEE Transactions on Robotics*, 24(1), 27–44.
- Canuto, C., Hussaini, M. Y., Quarteroni, A., & Zang, T. A. (2006). *Spectral methods*. Berlin: Springer.
- Ceylan, M., Henriques, D. Y. P., Tweed, D. B., & Crawford, J. D. (2000). Task-dependent constraints in motor control: pinhole goggles make the head move like an eye. *The Journal of Neuroscience*, 20(7), 2719–2730.
- Donders, F. C. (1848). Beiträge zur lehre von den bewegungen des menschlichen auges. *Holländische Beiträge zu den Anatomischen und Physiologischen Wissenschaften*, 1, 104–145. Press, 1996.
- Dunn, F., & Parberry, I. (2011). *3D math primer for graphics and game development* (2nd ed.). Boca Raton, London, New York: CRC Press, Taylor and Francis Group (Hardcover).
- Fahroo, F., & Ross, I. (2001). Costate estimation by a Legendre pseudospectral method. *Journal of Guidance, Control, and Dynamics*, 24, 270–277.
- Feldman, A. G., & Latash, M. (2005). Testing hypotheses and the advancement of science: recent attempts to falsify the equilibrium point hypothesis. *Experimental Brain Research*, 161, 91–103.
- Fick, A. (1858). Neue versuche über die augenstellungen. *Untersuchungen zur Naturlehre des Menschen*, 193.
- Fox, C. (2010). *An introduction to the calculus of variations*. Oxford University Press (Hardcover), 1954. Dover Publications (Paperback).
- Ghosh, B. K., & Wijayasinghe, I. (2012). Dynamics of human head and eye rotations under Donders' constraint. *IEEE Transactions on Automatic Control*, 57(10), 2478–2489.
- Glaser, S., Hoshi, M., Kempermann, U., Eggert, T., & Büttner, U. (2003). Three dimensional eye position and slow phase velocity in humans with downbeat nystagmus. *Journal of Neurophysiology*, 89, 338–354.
- Glenn, B., & Vilis, T. (1992). Violations of listing's law after large eye and head gaze shifts. *Journal of Neurophysiology*, 68, 309–318.
- Gomi, H., & Kawato, M. (1996). Equilibrium-point control hypothesis examined by measured arm-stiffness during multi-joint movement. *Science*, 272, 117–120.
- Kardamakis, A. A., & Moschovakis, A. K. (2009). Optimal control of gaze shifts. *The Journal of Neuroscience*, 29(24), 7723–7730.
- Kremmyda, O., Glasauer, S., Guerrasio, L., & Büttner, U. (2011). Effects of unilateral midbrain lesions on gaze (eye and head) movements. *Annals of the New York Academy of Sciences*, 1233, 71–77.
- Listing, J. B. (1845). *Beiträge zur physiologischen optik, göttinger studien*. Göttingen: Vandenhoeck und Ruprecht.
- Medendorp, W. P., Melis, B. J. M., Gielen, C. C. A. M., & Gisbergen, J. A. M. V. (1998). Off-centric rotation axes in natural head movements: implications for vestibular reafference and kinematic redundancy. *Journal of Neurophysiology*, 79, 2025–2039.
- Misslisch, H., Tweed, D., & Vilis, T. (1998). Neural constraints on eye motion in human eye-head saccades. *Journal of Neurophysiology*, 79, 859–869.
- O'Reilly, O. M. (2008). *Intermediate dynamics for engineers: an unified treatment of Newton-Euler and Lagrangian mechanics*. Cambridge, New York, Melbourne, Madrid, CapeTown, Singapore, Sao Paulo, Delhi: Cambridge University Press (Hardcover).
- Polpitiya, A. D., Dayawansa, W. P., Martin, C. F., & Ghosh, B. K. (2007). Geometry and control of human eye movements. *IEEE Transactions on Automatic Control*, 52(2), 170–180.
- Pontryagin, L. S., Boltyanskii, V. G., Gamkrelidze, R. V., & Mishchenko, E. F. (1962). *The mathematical theory of optimal processes*. New York: John Wiley & Sons.
- Radau, P., Tweed, D., & Vilis, T. (1994). Three dimensional eye head and chest orientations following large gaze shifts and the underlying neural strategies. *Journal of Neurophysiology*, 72, 2840–2852.
- Ruths, J., & Li, J.-S. (2011). A multidimensional pseudospectral method for optimal control of quantum ensembles. *The Journal of Chemical Physics*, 134, 044128.
- Smith, S. (2006). Lebesgue constants in polynomial interpolation. *Annales Mathematicae et Informaticae*, 33, 109–123.
- Stefanatos, D., Ruths, J., & Li, J.-S. (2010). Frictionless atom cooling in harmonic traps: a time-optimal control approach. *Physical Review A*, 82, 063422.
- Straumann, D., Haslwanter, T., Hepp-Reymond, M. C., & Hepp, K. (1991). Listing's law for the eye, head, and arm movements and their synergistic control. *Experimental Brain Research*, 86, 209–215.
- Theeuwes, M., Miller, L. E., & Gielen, C. C. A. M. (1993). Are the orientations of the head and arm related during pointing movements? *Journal of Motor Behavior*, 25, 242–250.
- Tweed, D., Glenn, B., & Vilis, T. (1995). Eye-head coordination during large gaze shifts. *Journal of Neurophysiology*, 73, 766–779.
- Tweed, D., Haslwanter, T., & Fetter, M. (1998). Optimizing gaze control in three dimensions. *Science*, 281(28), 1363–1365.
- Tweed, D., & Vilis, T. (1987). Implications of rotational kinematics for the oculomotor system in three dimensions. *Journal of Neurophysiology*, 58, 832–849.

von Helmholtz, H. (1866). *Handbuch der physiologischen optik. Number 3, Leopold Voss, Hamburg & Leipzig, 1910* (3rd ed.). Leipzig: Vos.



Indika Wijayasinghe is a visiting Assistant Professor in the Department of Mathematics and Statistics at Sam Houston State University, Huntsville, TX. He received his B.Sc. in electrical and electronics engineering from the University of Peradeniya, Sri Lanka, in 2007 and Ph.D. in applied mathematics from Texas Tech University, Lubbock, TX, USA, in 2013. His research interests are in Control Theory and BioMechanics.



Justin Ruths received the B.S. from Rice University, Houston, TX, USA, the M.S. from Columbia University, New York, NY, USA, and the Ph.D. degree in systems science and applied mathematics from Washington University, St. Louis, MO, USA. He is currently an Assistant Professor at the Singapore University of Technology and Design in the Engineering Systems and Design Pillar. His research interests are in the areas of computational optimal control theory, network science, and large-scale complex dynamical systems.



Ulrich Büttner is professor emeritus at the Department of Neurology, Ludwig-Maximilians-Universität München. Before his retirement he was the first director of the Bernstein Center for Computational Neuroscience (BCCN), Munich. His present work focuses on the recording, analysis and mathematical modeling of neuronal data from cortical neurons in the behaving monkey.



Bijoy K. Ghosh received his Ph.D. in engineering sciences from Harvard University, Cambridge, MA, in 1983. From 1983 to 2007 he was with the Department of Electrical and Systems Engineering, Washington University, St. Louis, MO, USA, as a Professor and the Director of the Center for BioCybernetics and Intelligent Systems. Currently he is the Dick and Martha Brooks Regents Professor of Mathematics and Statistics at Texas Tech University, Lubbock, TX, USA. Bijoy's research interests are in Control Theory and Biomechanics.



Stefan Glasauer is an Associate Professor at the Institute of Clinical Neurosciences and heads the Sensorimotor Research Center at the Ludwig-Maximilians-Universität München. He serves as deputy director of the German Center for Vertigo and Balance Disorders and is member of the Bernstein Center for Computational Neuroscience Munich. His group focuses on the Analysis and Mathematical Modeling of Human Perception and Sensorimotor Behavior.



Olympia Kremmyda studied medicine in the University of Athens, Greece, where she also earned her Ph.D. She currently works as a Neurologist in the Department of Neurology of the University of Munich. Her scientific interests include Eye and Head Coordination in midbrain and cerebellar patients, as well as Three Dimensional Eye Movements in patients with acute and chronic brainstem and cerebellar lesions.



Jr-Shin Li received his B.S. and M.S. degrees from National Taiwan University and his Ph.D. degree in applied mathematics from Harvard University in 2006. He is currently an Associate Professor in electrical and systems engineering with a joint appointment in the Division of Biology & Biomedical Sciences at Washington University in St. Louis. His research interests are in the areas of Control Theory, Computational Mathematics, and Optimization.